ACCOUNTS of chemical research

Article

pubs.acs.org/accounts

Preparation and Applications of Mechanically Exfoliated Single-Layer and Multilayer MoS_2 and WSe_2 Nanosheets

Hai Li, Jumiati Wu, Zongyou Yin, and Hua Zhang*

School of Materials Science and Engineering, Nanyang Technological University, 50 Nanyang Avenue, Singapore 639798, Singapore

CONSPECTUS: Although great progress has been achieved in the study of graphene, the small current ON/OFF ratio in graphene-based field-effect transistors (FETs) limits its application in the fields of conventional transistors or logic circuits for low-power electronic switching. Recently, layered transition metal dichalcogenide (TMD) materials, especially MoS_2, have attracted increasing attention. In contrast to its bulk material with an indirect band gap, a single-layer (1L) MoS_2 nanosheet is a semiconductor with a direct band gap of ~1.8 eV, which makes it a promising candidate for optoelectronic applications due to the enhancement of photoluminescence and high current ON/OFF ratio.

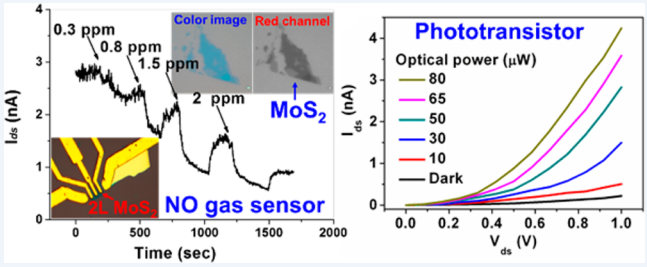

Compared with TMD nanosheets prepared by chemical vapor deposition and liquid exfoliation, mechanically exfoliated ones possess pristine, clean, and high-quality structures, which are suitable for the fundamental study and potential applications based on their intrinsic thickness-dependent properties. In this Account, we summarize our recent research on the preparation, characterization, and applications of 1L and multilayer MoS_2 and WSe_2 nanosheets produced by mechanical exfoliation. During the preparation of nanosheets, we proposed a simple optical identification method to distinguish 1L and multilayer MoS_2 and WSe_2 nanosheets on a Si substrate coated with 90 and 300 nm SiO_2. In addition, we used Raman spectroscopy to characterize mechanically exfoliated 1L and multilayer WSe_2 nanosheets. For the first time, a new Raman peak at 308 cm^{-1} was observed in the spectra of WSe_2 nanosheets except for the 1L WSe_2 nanosheet. Importantly, we found that the 1L WSe_2 nanosheet is very sensitive to the laser power during characterization. The high power laser-induced local oxidation of WSe_2 nanosheets and single crystals was monitored by Raman spectroscopy and atomic force microscopy (AFM). Hexagonal and monoclinic structured WO_3 thin films were obtained from the local oxidization of single- to triple-layer (1L-3L) and quadruple- to quintuple-layer (4L-5L) WSe_2 nanosheets, respectively. Then, we present Raman characterization of shear and breathing modes of 1L and multilayer MoS_2 and WSe_2 nanosheets in the low frequency range (<50 cm^{-1}), which can be used to accurately identify the layer number of nanosheets. Magnetic force microscopy was used to characterize 1L and multilayer MoS_2 nanosheets, and thickness-dependent magnetic response was found. In the last part, we briefly introduce the applications of 1L and multilayer MoS_2 nanosheets in the fields of gas sensors and phototransistors.

1. INTRODUCTION

Graphene, a two-dimensional (2D), one-atom-thick, and single-layer (1L) carbon material, has received great interest due to its fascinating properties, such as ultrahigh carrier mobility, good thermal conductivity, and excellent mechanical property.[1,2] However, because of its gapless band structure, the small current ON/OFF ratio in graphene-based field effect transistors (FETs) makes it difficult to use them for conventional transistors or logic circuits for low-power electronic switching at room temperature.[3,4] Many techniques have been tried to modulate the band gap of graphene, such as chemical functionalization of graphene, application of high electric field on graphene, or preparation of graphene nanoribbons. However, the aforementioned modifications might result in the loss of mobility or increase of experimental complexity.[3] Inspired by the great advances of graphene research, layered transition metal dichalcogenide (TMD) materials with band gaps around 1−2 eV have attracted increasing attention in recent years.[3−6]

During the last decades, TMDs have been extensively used in the applications of lubrication, catalysis, energy storage, and photovoltaics.[3,5] When the size of TMDs decreases from three dimensions to two dimensions, interesting layer-dependent properties are found in atomically thin TMD nanosheets compared with their bulk compounds, which are attributed to the quantum confinement and surface effects.[3−12] For example, some bulk TMDs are semiconductors with indirect band gaps, while their 1L nanosheets are semiconductors with direct band gaps, resulting in the dramatic properties such as the enhancement of photoluminescence.[7,13,14] Valley polarization was also found in the 1L MoS_2 nanosheet but not in the double-layer (2L) MoS_2 nanosheet.[15,16]

Very recently, atomically thin 2D TMD nanosheets have exhibited extensive applications in transistors, sensors, memory devices, and optoelectronic devices.[13,17−35] Similar to graphite, the MoS_2 bulk crystal is naturally abundant. Therefore, a mechanical exfoliation method has been used to prepare atomically thin MoS_2 nanosheets for various applica-

Received: September 27, 2013
Published: April 3, 2014

   dx.doi.org/10.1021/ar4002312 | Acc. Chem. Res. 2014, 47, 1067−1075

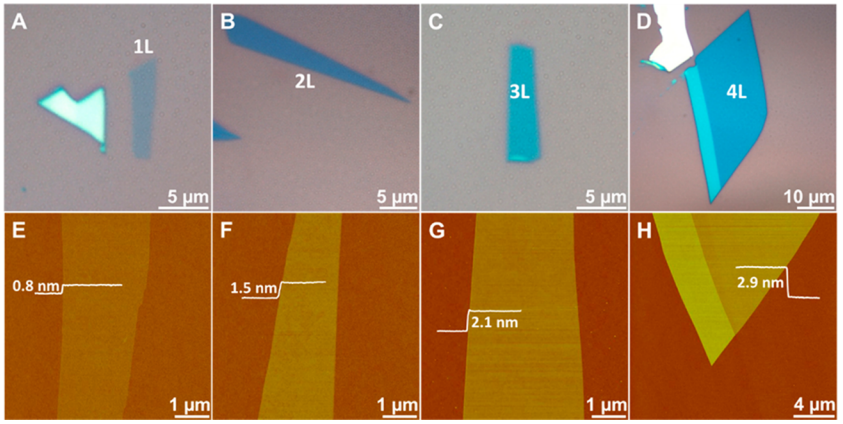

Figure 1. Mechanically exfoliated single- and few-layer MoS_2 nanosheets on 300 nm SiO_2/Si. Optical microscopy (A–D) and AFM (E–H) images of single-layer (1L, thickness 0.8 nm; A and E), double-layer (2L, thickness 1.5 nm; B and F), triple-layer (3L, thickness 2.1 nm; C and G), and quadruple-layer (4L, thickness 2.9 nm; D and H) MoS_2 nanosheets. Reprinted with permission from ref 18. Copyright 2012 Wiley-VCH Verlag GmbH & Co.

tions.[5,7,8,10,12−21,36,37] Among the other TMD crystals, WSe_2 is one of the most widely studied materials due to the easy synthesis and tunable doping behavior of its bulk crystal. The study of WSe_2 bulk crystal is mainly focused on the photovoltaic application in the conversion of solar energy into electricity and photoelectrochemical hydrogen production.[38,39] However, only a few of studies focus on the characterization and applications of mechanically exfoliated single-layer to multilayer WSe_2 nanosheets.[8,40−44]

Many methods have been reported to prepare the atomically thin MoS_2 and WSe_2 nanosheets, including mechanical exfoliation,[5,8,13−18,20,36,40,41−43] chemical exfoliation,[11,35] chemical vapor deposition,[45] and sonication.[46] Although its scale-up is limited, the mechanical exfoliation is still a powerful method to fabricate atomically thin 2D layered nanosheets for investigation of their intrinsic thickness-dependent properties. In this Account, we focus on the preparation, characterization, and applications of the mechanically exfoliated MoS_2 and WSe_2 nanosheets.

2. PREPARATION AND CHARACTERIZATION OF SINGLE-LAYER AND MULTILAYER MoS_2 AND WSe_2 NANOSHEETS

2.1. Preparation of Single-Layer and Multilayer MoS_2 and WSe_2 Nanosheets by Mechanical Exfoliation

To date, mechanical exfoliation is the most efficient way to produce the cleanest, highly crystalline and atomically thin nanosheets of layered materials. In a typical mechanical exfoliation process, appropriate thin TMD crystals are first peeled off from their bulk crystals by using adhesive Scotch tape. These freshly cleaved thin crystals on Scotch tape are brought into contact with a target substrate and rubbed by using tools such as plastic tweezers to further cleave them. After the Scotch tape is removed, 1L and multilayer TMD nanosheets are left on the substrate. As shown in Figure 1, 1L to quadruple-layer (4L) MoS_2 nanosheets with clean surfaces were deposited on Si substrates with 300 nm SiO_2 coating layer (referred to as 300 nm SiO_2/Si).[18] AFM measurement indicates that the heights of 1L–4L MoS_2 nanosheets are 0.8, 1.5, 2.1, and 2.9 nm, respectively.

2.2. Optical Identification of Single-Layer and Multilayer MoS_2 Nanosheets

By use of the mechanical exfoliation method, not only 1L and multilayer MoS_2 nanosheets but also a large quantity of thicker and bulk-like MoS_2 flakes are left on the substrate. Therefore, how to locate and identify the 1L and multilayer MoS_2 nanosheets in a rapid and accurate way is the first step prior to the fundamental research and practical applications. Recently, we have developed a simple, rapid, and reliable optical method to identify the single- to quindecuple-layer (1L–15L) 2D nanosheets, such as graphene, MoS_2, WSe_2, and TaS_2, on 90 or 300 nm SiO_2/Si.[47] Taking MoS_2 nanosheet on 90 nm SiO_2/Si as an example (Figure 2A), the optical contrast of the MoS_2 nanosheet

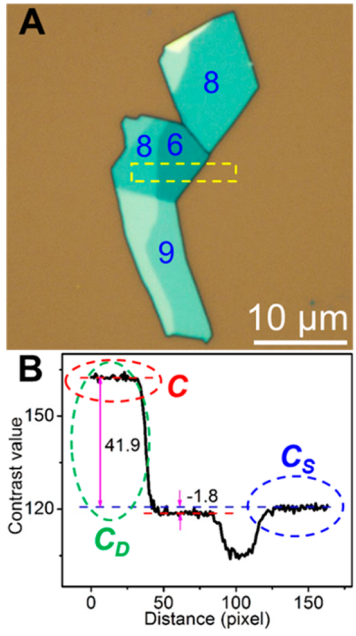

Figure 2. (A) Color optical image of a MoS_2 flake deposited on 90 nm SiO_2/Si. The digits indicate the layer numbers of MoS_2 nanosheets. (B) Contrast profile of the dashed rectangle shown in panel A. Reprinted with permission from ref 47. Copyright 2013 American Chemical Society.

and substrate are defined as C and C_S (Figure 2B), respectively, which were measured from its color optical image by using ImageJ.[48] The contrast difference between MoS_2 and substrate is defined as C_D (Figure 2B). By measuring the C_D values of MoS_2 nanosheets with different layer numbers, we generated a standard chart of C_D values vs layer number (Figure 3A), which can be

dx.doi.org/10.1021/ar4002312 | Acc. Chem. Res. 2014, 47, 1067−1075

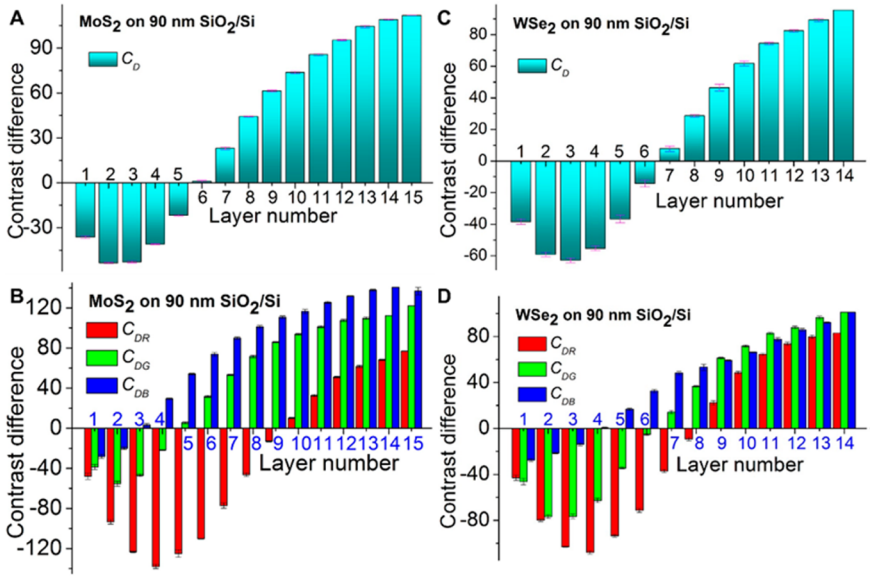

Figure 3. Plot of C_D values (A, C) and C_{DR}, C_{DG}, and C_{DB} values (B, D) of 1L−15L MoS_2 (A, B) and 1L−14L WSe_2 (C, D) nanosheets on 90 nm SiO_2/Si. Reprinted with permission from ref 47. Copyright 2013 American Chemical Society.

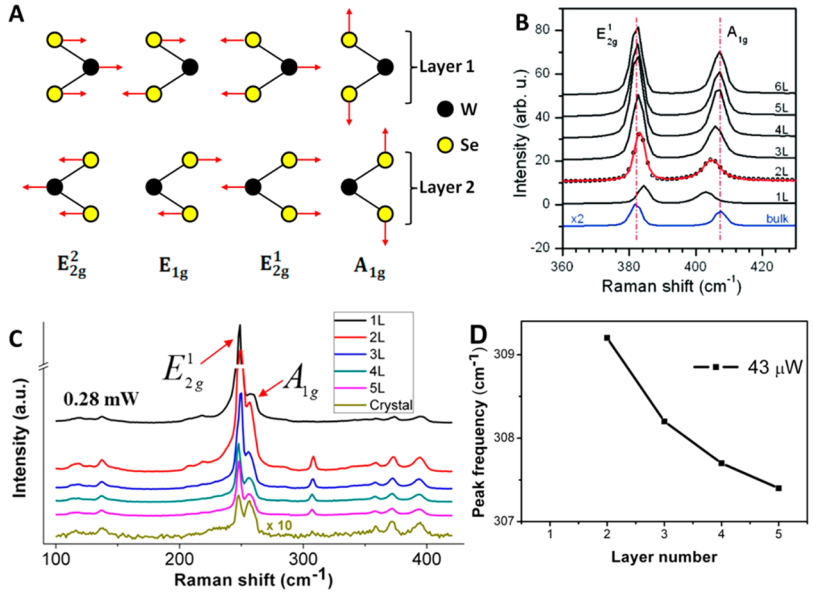

Figure 4. (A) Atomic displacements of the four Raman-active modes in the unit cell of the bulk WSe_2 crystal. (B) Raman spectra of 1L−6L MoS_2 nanosheets and bulk crystal. (C) Raman spectra of 1L−5L WSe_2 nanosheets and bulk crystal at laser excitation power of 0.28 mW. (D) Peak frequencies of the Raman peak near 308 cm^{-1} as a function of layer number of WSe_2 at laser excitation power of 43 μW. Reprinted with permission from refs 40 and 49. Copyright 2012 Wiley-VCH Verlag GmbH & Co and 2010 American Chemical Society.

readily used to determine the thickness of MoS_2 nanosheets on 90 nm SiO_2/Si.

However, the C_D values of 1L and 4L MoS_2 nanosheets as well as 2L and 3L MoS_2 nanosheets on 90 nm SiO_2 substrate are indistinguishable (Figure 3A). In order to reliably distinguish MoS_2 nanosheets on 90 nm SiO_2/Si, the color optical image of the MoS_2 nanosheet is split into the grayscale red (R), green (G), and blue (B) channel images using the ImageJ.[48] The contrast difference between the MoS_2 nanosheet and substrate in R, G, or B channel is defined as C_{DR}, C_{DG} or C_{DB}, respectively. By measuring the C_{DR}, C_{DG} and C_{DB} values, 1L−15L MoS_2 nanosheets on 90 nm SiO_2/Si can be reliably identified (Figure 3B). Similarly, 1L−14L WSe_2 nanosheets on 90 nm SiO_2/Si can also be reliably identified by measuring the C_D, C_{DR}, C_{DG}, and C_{DB} values (Figure 3C,D). In addition, 1L−15L MoS_2 and 1L−14L WSe_2 nanosheets on 300 nm SiO_2/Si can also be identified by using this optical method.[47]

2.3. Raman Characterization of Single-Layer and Multilayer MoS_2 and WSe_2 Nanosheets

Raman spectroscopy has been widely used to characterize structural and electronic properties of 2D layered nanomaterials. It is also an effective technique for the rapid identification and characterization of MoS_2 and WSe_2 nanosheets.[8,40,44,49,50] As shown in Figure 4A, MoS_2 and WSe_2 bulk crystals usually have four Raman active modes, E^2_{2g}, E_{1g}, E^1_{2g}, and A_{1g}.[40] Due to the selection rules in the backscattering geometry, the E_{1g} mode is hardly observed. In addition, the low-energy E^2_{2g} mode is difficult to detect with the common commercial instrument because of

dx.doi.org/10.1021/ar4002312 | Acc. Chem. Res. 2014, 47, 1067−1075

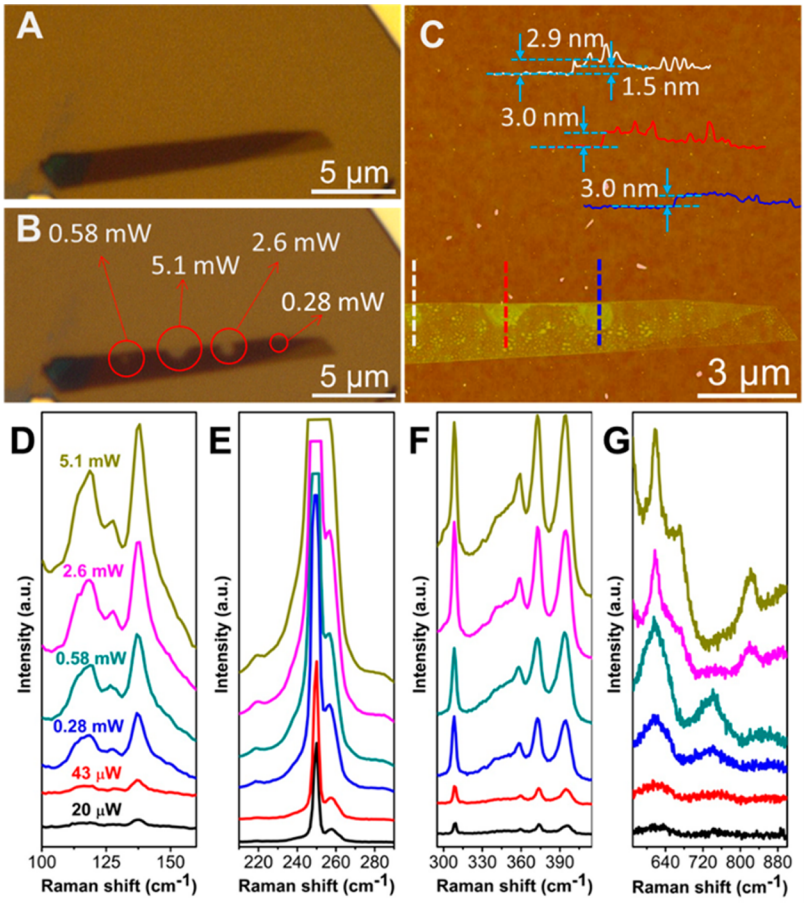

Figure 5. Optical images of 2L WSe_2 nanosheets before (A) and after (B) Raman characterization. The red circles shown in panel B indicate spots where the Raman spectra were recorded. (C) The corresponding AFM image of panel B. Inset, height profiles of spots. (D−G) Raman spectra of 2L WSe_2 nanosheets in the range of (D) 100−160 cm^{-1}, (E) 210−290 cm^{-1}, (F) 295−415 cm^{-1}, and (G) 570−900 cm^{-1} with laser excitation power increased from 20 μW to 5.1 mW. Reprinted with permission from ref 40. Copyright 2013 Wiley-VCH Verlag GmbH & Co.

the limited rejection of the Rayleigh scattering.[8,49] Therefore, a special notch filter is necessary to detect the E^2_{2g} mode.[8] The E^1_{2g} and A_{1g} modes of 1L MoS_2 nanosheets are located at ∼384 and 403 cm^{-1}, respectively.[18,36,49] Red shift of the E^1_{2g} mode and blue shift of the A_{1g} mode were observed with increase of the layer number of MoS_2 nanosheets from 1L−4L (Figure 4B).[49] There is no obvious difference in Raman spectra between MoS_2 nanosheets thicker than 4L and bulk crystal.

In contrast to MoS_2, there are some second order and combinational modes in addition to E^1_{2g} and A_{1g} modes in the Raman spectrum of WSe_2 bulk crystal (Figure 4C).[40] Two strong peaks around 250 cm^{-1} are assigned to E^1_{2g} and A_{1g} modes, respectively. Interestingly, the peak at 308 cm^{-1} is absent in 1L WSe_2 nanosheet and becomes Raman active in 2L and thicker WSe_2 nanosheets,[8,40] which can be used to quickly identify 1L WSe_2 nanosheet. The Raman peaks at 308 cm^{-1} red shift with the increasing layer number (Figure 4D), which might reflect the presence of additional interlayer interactions.

It is well-known that laser-induced local heating will affect the Raman characterization of materials. Although MoS_2 bulk crystal is stable even when exposed to a laser power of 6.3 mW, a laser power of 10 mW can induce thinning of multilayer MoS_2 down to 1L.[37] However, we found that WSe_2 bulk crystal and nanosheets are very sensitive to laser-induced local heating.[40]

WSe_2 bulk crystal undergoes laser-assisted oxidization when exposed to a laser power of 2.6 mW.[40] The oxidization of 2L WSe_2 nanosheets occurs when they are exposed to a laser power of 0.58 mW (Figure 5A, B), which can be clearly observed by optical microscopy (Figure 5B) and AFM measurements (Figure 5C). As the laser power increased from 20 μW to 0.28 mW, the intensities of Raman peaks kept increasing but no notable shift was observed (Figure 5D−F). When the laser power was increased from 0.58 to 5.1 mW, a new peak appearing at 822 cm^{-1} was observed (Figure 5G), which is attributed to the formation of hexagonal WO_3.[40,51]

The evolution of 1L WSe_2 nanosheets to hexagonal WO_3 is further monitored by the Raman and AFM measurements. As shown in Figure 6A, the thickness of a 1L WSe_2 nanosheet is ∼0.7 nm. After the nanosheet is exposed to a 488 nm laser with an excitation power of 0.7 mW for Raman mapping, the laser-induced oxidization starts from the edge of the 1L WSe_2 nanosheet, indicating that the edge is highly defective. As shown in Figure 6B, the height of edges increased to ∼2.4 nm after oxidization, which is consistent with the height of a triangular WO_3 film formed by electrochemical oxidization of WSe_2 bulk crystal.[52] The formed WO_3 film shows structures with 60° or 120° angles, indicating the formation of hexagonal WO_3, which is consistent with the Raman measurement. The central area of the 1L WSe_2 nanosheet remains intact after the first round of Raman mapping (Figure 6B), which indicates the smooth and defect-free vdW face of the mechanically exfoliated WSe_2 nanosheet. It has been reported that a defect-free van der Waals (vdW) face of WSe_2 is inert to the oxidization.[53] More structures with angles of 60° or 120° and height of 2.4 nm

dx.doi.org/10.1021/ar4002312 | Acc. Chem. Res. 2014, 47, 1067−1075

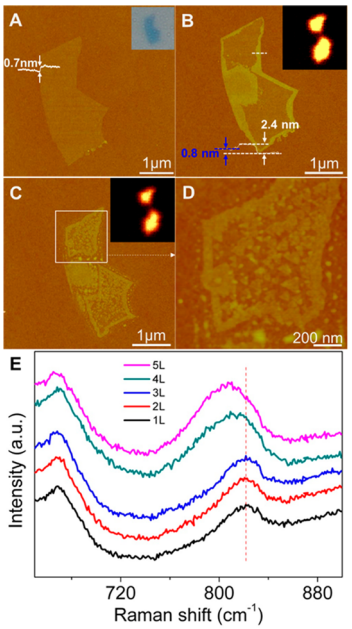

Figure 6. AFM images of 1L WSe_2 nanosheet before (A) and after the first (B) and second (C,D) rounds of oxidization by a laser with high excitation power of 0.7 mW. Inset in panel A is the optical image. Bottom inset in panel B shows the height profile of the white dashed line. Top right insets in panels B and C are the corresponding Raman mapping images. (D) AFM image of the white square in panel C. (E) Raman spectra of 1L−5L WSe_2 nanosheets oxidized by a laser with high excitation power in the range of 650−900 cm^{-1}. Reprinted with permission from ref 40. Copyright 2013 Wiley-VCH Verlag GmbH & Co.

appeared in the WSe_2 nanosheet surface after the second round of Raman mapping (Figure 6C,D), further confirming the formation of a hexagonal WO_3 film by laser-induced oxidization. Moreover, the oxidization of 2L−5L WSe_2 nanosheets was also studied using the Raman and AFM measurements. Similar to 1L WSe_2, hexagonal structured WO_3 films were found on 2L and 3L WSe_2 nanosheets after they were exposed to the laser with high power in ambient conditions, while monoclinic structured WO_3 films were found on 4L and 5L WSe_2 nanosheets.[40] The oxidization of 1L−5L WSe_2 nanosheets was also confirmed by Raman characterization. As shown in Figure 6E, the Raman peaks appeared at 822, 822, 822, 811, and 807 cm^{-1} for 1L, 2L, 3L, 4L, and 5L WSe_2 nanosheets, respectively, after they were exposed to the laser with high power in ambient conditions. The peak around 820 cm^{-1} is attributed to the hexagonal WO_3, while the peak around 810 cm^{-1} is attributed to the monoclinic WO_3.[40,51]

2.4. Low-Frequency Raman Characterization of Single-Layer and Multilayer MoS_2 and WSe_2 Nanosheets

In the low-frequency Raman spectrum range (<50 cm^{-1}), we have observed two thickness-dependent modes in multilayer MoS_2 and WSe_2 nanosheets, that is, shear (E^2_{2g}) and breathing (B^2_{2g}) modes.[8] The shear mode originates from in-plane oscillation of adjacent layers, which is parallel to the layer plane and also observed in bulk MoS_2, while the optically inactive breathing mode comes from the interlayer out-of-plane oscillation, which is perpendicular to the layer plane and not observed in bulk MoS_2.

As shown in Figure 7A, no rigid-layer vibration is observed in 1L MoS_2, which confirms the shear and breathing modes as interlayer vibrational modes. The strongest peak with a narrow bandwidth, that is, the E^2_{2g} mode (labeled as S1), undergoes a blue shift from 2L (~22 cm^{-1}) to 12L (~32 cm^{-1}) MoS_2 nanosheets.[8] There is almost no shift of the S1 peak from 12L MoS_2 nanosheet to bulk crystal, while the second strongest peak with a broad bandwidth, that is, B^2_{2g} mode (labeled as B1), undergoes a red shift from 2L (~40 cm^{-1}) to 9L (~10 cm^{-1}) MoS_2 nanosheets. The B1 peak is further red-shifted to ~5 cm^{-1} as the thickness of MoS_2 nanosheet increases to 19L,[54] which is out of the detection limit of our instrument. Moreover, two weak peaks labeled as S2 (shear mode) and B2 (breathing mode) are also observed for MoS_2 nanosheets thicker than 4L and 3L, respectively. Similarly, S2 peak undergoes a blue shift, while B2 peak undergoes a red shift with increased thickness (Figure 7A,B).

In terms of WSe_2, the same Raman-active modes with similar trends of evolution versus thickness is observed (Figure 7C,D), except that the frequencies of Raman modes are lower in WSe_2 compared with those of MoS_2. In addition, the B2 peak in WSe_2 is much stronger than that of MoS_2. As shown in Figure 7B,D, the breathing modes (B1 and B2 peaks) are strongly suppressed in the $\bar{z}(xy)z$ polarization, which is in agreement with the Raman selection rules for breathing modes.[8,54] Importantly, the aforementioned thickness-dependent Raman modes in low frequency range can be used for the accurate thickness identification of MoS_2 and WSe_2 nanosheets.

The atomically thin 2D nanosheets usually show novel physical properties compared with their bulk materials.[3−12] The MoS_2 crystal is nonmagnetic. However, it has been reported that the MoS_2 nanosheet with typical edge dimension of ~100 nm has shown weak magnetism, which might be attributed to the existence of the zigzag edges in the ferromagnetic ground state.[55] In our magnetic force microscopy (MFM) study, we found that the magnetic response of MoS_2 nanosheets is thickness-dependent, that is, the increase of magnetic signal has been observed in MoS_2 thin flake as its thickness decreased.[12]

3. APPLICATIONS OF SINGLE-LAYER AND MULTILAYER MoS_2 NANOSHEETS BASED DEVICES

3.1. Gas Sensors

Compared with a 1D semiconductor, the 2D configuration of graphene nanosheets enables better adsorption of gas molecules and thus leads to lower electrical noise and better detection limit. As the semiconducting analogue of graphene, the MoS_2 nanosheet is expected to be a potential candidate for gas sensing applications.

As a proof of concept, MoS_2 field-effect transistor (FET) devices were fabricated with mechanically exfoliated 1L−4L MoS_2 nanosheets as channels and used to detect NO gas at room temperature.[18] MoS_2 FETs fabricated with 2L−4L MoS_2 nanosheets exhibited better performance compared with the 1L MoS_2 nanosheet-based device, which showed rapid but unstable response. Figure 8A shows the current response of a 2L MoS_2 nanosheet-based FET device upon exposure to NO with concentrations ranging from 0.3 to 2 ppm. When the device was exposed to NO gas, the current dropped quickly for the first stage (~30 s) and then continuously decreased for more than 2 min until the saturation of NO adsorption was achieved (top right inset in Figure 8A). Due to the strong adsorption of NO on the MoS_2 surface, complete desorption of adsorbed NO molecules was very slow. A plot of percent change in the current of 2L MoS_2 FET as a function of NO concentration is shown in Figure 8B. The detection limit of 2L MoS_2 FET was 0.8 ppm NO, at which the signal-to-noise ratio is approximately 3. Our results indicate

dx.doi.org/10.1021/ar4002312 | Acc. Chem. Res. 2014, 47, 1067−1075

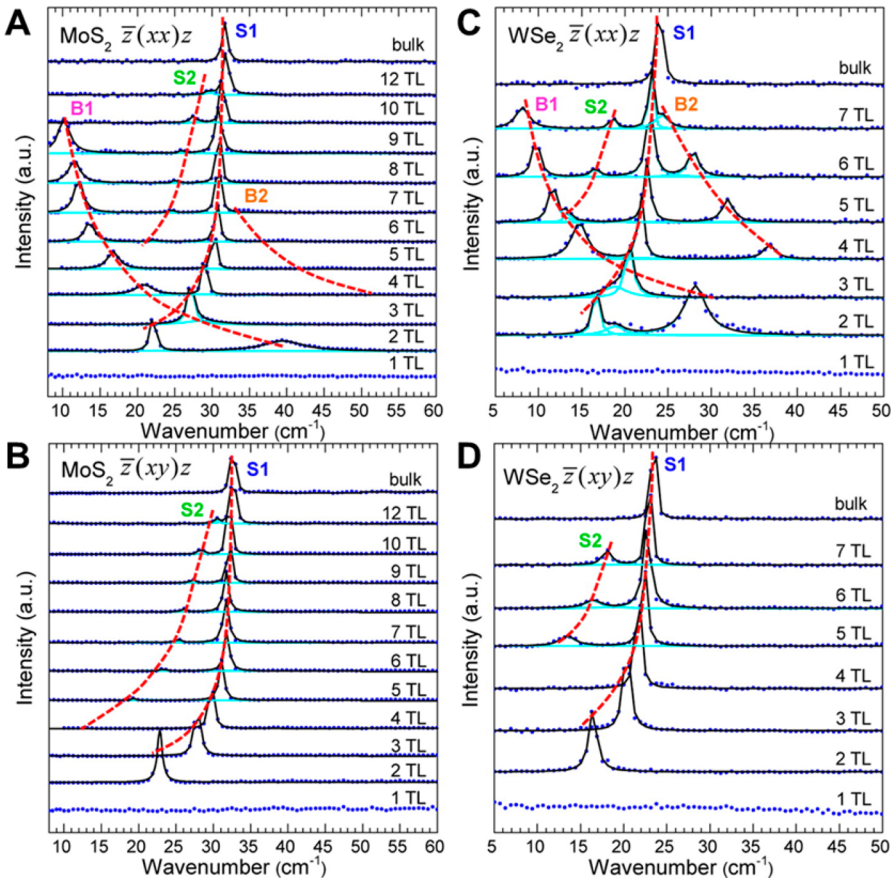

Figure 7. The shear and breathing modes evolutions as a function of layer number of MoS_2 and WSe_2 nanosheets in low-frequency Raman spectra. (A, B) Low-frequency Raman spectra of 1L−12L MoS_2 nanosheets measured using the $\bar{z}(xx)z$ polarization configuration (A) and the $\bar{z}(xy)z$ polarization configuration (B), respectively. (C, D) Low-frequency Raman spectra of 1L−7L WSe_2 nanosheets measured under the $\bar{z}(xx)z$ polarization configuration (C) and $\bar{z}(xy)z$ polarization configuration (D), respectively. The blue dots are experimental data points, while the black solid curves are Lorentzian fittings to the data. S1−S2 and B1−B2 represent the shear and breathing modes, respectively. Reprinted with permission from ref 8. Copyright 2013 American Chemical Society.

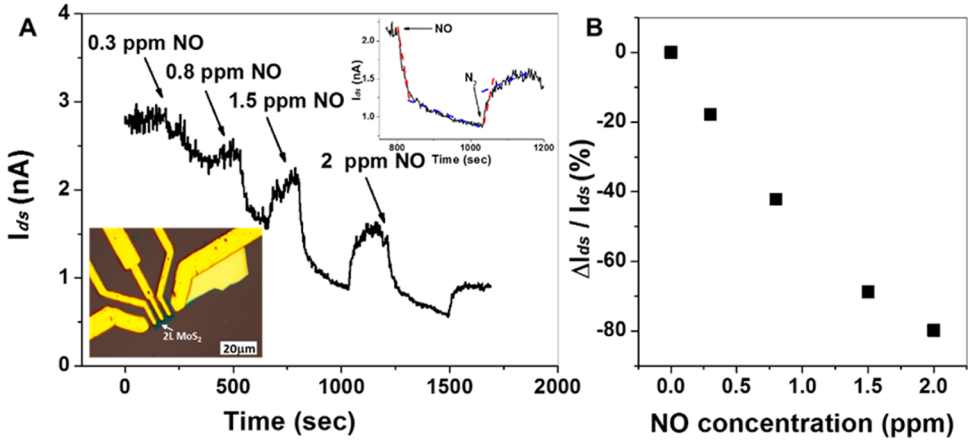

Figure 8. NO gas sensor based on a 2L MoS_2 FET device. (A) Real-time current response after exposure of the 2L MoS_2 FET to NO gas with increasing concentration. Bottom inset, optical image of the FET device. Top right inset, a typical adsorption and desorption process of NO with rapid (red dashed lines) and slow steps (blue dashed lines). (B) Plot of percentage change in current vs concentration of NO gas. Reprinted with permission from ref 18. Copyright 2012 Wiley-VCH Verlag GmbH & Co.

that the mechanically exfoliated multilayer MoS_2 nanosheets are promising channel materials for potential gas sensors.

3.2. Phototransistors

Bulk MoS_2 is a semiconductor with an indirect band gap of 1.3 eV, while a transition from indirect to direct band gap is observed when the thickness of MoS_2 is single-layer.[7] This unique characteristic of 1L MoS_2 nanosheet is expected to result in outstanding optoelectronic properties, which inspires the research on its related optoelectronic device applications. Our group first developed a highly photoresponsive transistor based

dx.doi.org/10.1021/ar4002312 | Acc. Chem. Res. 2014, 47, 1067−1075

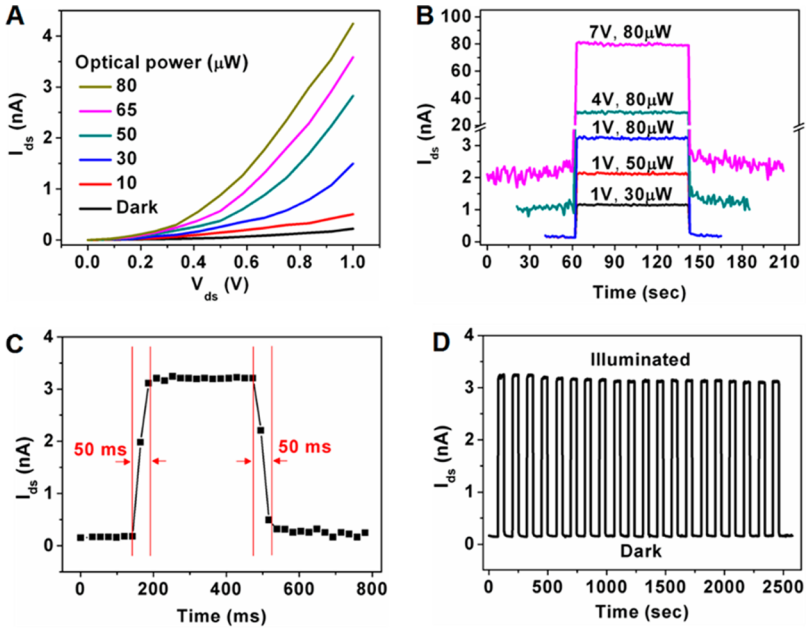

Figure 9. Electrical characteristics of a single-layer MoS_2 nanosheet based phototransistor. (A) Typical output characteristics of phototransistor at different illuminating optical power (10−80 μW) at V_g = 0 V. (B) Photoswitching characteristics of a single-layer MoS_2 phototransistor at different optical power (P_{light}) and drain voltage (V_{ds}). (C) Photoswitching rate and (D) stability test of photoswitching behavior of a single-layer MoS_2 phototransistor at V_{ds} = 1 V, P_{light} = 80 μW. Reprinted with permission from ref 13. Copyright 2012 American Chemical Society.

on 1L MoS_2 with 300 nm SiO_2 as the bottom dielectric layer on the Si substrate.[13] As shown in Figure 9A, the photocurrent of the 1L MoS_2 phototransistor increases with the incident optical power within the whole range of applied drain voltage (0−1 V). Figure 9B further indicates the dependence of photocurrent on the optical power and drain voltage, which demonstrates that the photocurrent from the 1L MoS_2 phototransistor can be well controlled by the illuminated optical power and applied drain voltage. Prompt photocurrent generation and annihilation (also called photoswitching) behavior is observed and can be completely switched between ON and OFF states within ca. 50 ms by manipulating the incident light (Figure 9C). Moreover, the 1L MoS_2 phototransistor exhibits quite stable characteristics. As shown in Figure 9D, applying multiple periodic illumination−dark cycles on the device can consistently switch it ON and OFF. Impressively, with constant incident optical power of 80 μW and drain voltage at 1 V, the photoresponsivity of our 1L MoS_2 phototransistor reaches 7.5 mA/W at the applied gate voltage of ∼50 V. It is higher than that of a graphene-based device, which is ∼1 mA/W at the applied gate voltage of 60 V.[56]

Several following studies on phototransistors based on mechanically exfoliated MoS_2 nanosheets were also reported from other research groups. By using ITO as top gate electrode and 50 nm thick Al_2O_3 on top of MoS_2 as the dielectric layer, Lee et al. fabricated transparent top-gate phototransistors based on mechanically exfoliated 1L−3L MoS_2 nanosheets.[20] They found that 1L and 2L MoS_2 nanosheets with band gaps of 1.8 and 1.65 eV, respectively, exhibit efficient detection for green light, while 3L MoS_2 with a band gap of 1.35 eV is more sensitive for red light detection. The average photoresponsivity of these devices can reach ∼100 mA/W under gate voltages from −7 to −10 V. A similar photoresponsivity was also obtained from a bottom-gate phototransistor based on mechanically exfoliated multilayer MoS_2, where atomic-layer-deposited (ALD) 50 nm thick Al_2O_3 was used as the bottom dielectric layer and the applied gate voltage was −3 V.[57] In the aforementioned reports, applying negative gate voltage brings the advantages of low dark current for the phototransistor, which lowers heat generation during the device operation.[20,57] Very recently, by carefully removing a thin (<5 nm) surface layer of the SiO_2 dielectric layer followed by the plasma treatment, the photoresponsivity of a bottom-gate phototransistor based on a single-layer MoS_2 nanosheet reached a new record of 880 A/W at gate voltage of −70 V, due to the improved mobility of the device.[14]

4. CONCLUSIONS AND OUTLOOK

In this Account, we summarized the preparation, characterization, and applications of single-layer and multilayer MoS_2 and WSe_2 nanosheets prepared by the mechanical exfoliation method. The obtained MoS_2 and WSe_2 nanosheets are suitable for fundamental study of their intrinsic thickness-dependent properties, such as band gap, mobility, and vibrational mode.

Some challenges still remain in the application of the mechanically exfoliated nanosheets. First, the mechanical exfoliation method needs large sized TMD bulk crystals in order to prepare nanosheets with suitable size for characterization and device fabrication. However, many TMD bulk crystals need to be synthesized by the chemical vapor transport (CVT) method, which is time-consuming and expensive. Second, mechanical exfoliation usually produces nonuniform flakes. Therefore, rapid determination of location and layer number of mechanically exfoliated nanosheets is very important.

Although many efforts are focused on mechanically exfoliated MoS_2 nanosheets, a few studies have been reported on mechanically exfoliated WSe_2 nanosheets. Interestingly, the pristine p-type WSe_2 nanosheet can be simply tuned to n-type by selecting a proper contact metal or doping the contacts accordingly.[42,43] We believe the fundamental study and potential applications of mechanically exfoliated 1L and multilayer MoS_2 and WSe_2 nanosheets in the fields of electronic devices, optoelectronics, integrated circuits, and sensors might open up an avenue for other TMD nanosheets.

dx.doi.org/10.1021/ar4002312 | Acc. Chem. Res. 2014, 47, 1067−1075

AUTHOR INFORMATION

Corresponding Author

*Tel: +65-67905175. Fax: +65-67909081. E-mail: hzhang@ntu.edu.sg, hzhang166@yahoo.com. Website: http://www.ntu.edu.sg/home/hzhang/.

Funding

This work was supported by MOE under AcRF Tier 2 (ARC 26/13, No. MOE2013-T2-1-034), AcRF Tier 1 (RG 61/12, RGT18/13, and RG5/13), and Start-Up Grant (M4080865.070.706022) in Singapore. This Research is also conducted by NTU-HUJ-BGU Nanomaterials for Energy and Water Management Programme under the Campus for Research Excellence and Technological Enterprise (CREATE), that is supported by the National Research Foundation, Prime Minister's Office, Singapore.

Notes

The authors declare no competing financial interest.

Biographies

Hai Li received his B.Sc. from Zhengzhou University, China (2001), and his Ph.D. from the Chinese Academy of Sciences (2007). He is currently working as a senior research fellow in Professor Hua Zhang's group. His research interests include the synthesis and applications of mechanically exfoliated two-dimensional nanomaterials.

Jumiati Wu obtained her B.Sc in Materials Science and Engineering from Nanyang Technological University, Singapore, in 2009. She is currently pursuing a Ph.D. under Prof. Hua Zhang's guidance since 2010. Her research interests include the synthesis and applications of mechanically exfoliated two-dimensional nanomaterials.

Zongyou Yin studied at Jilin University in China for his B.E. and M.S. and completed his Ph.D. at Nanyang Technological University in Singapore (2008). He is currently working as a senior research fellow in Prof. Hua Zhang's group. His research interests include the synthesis and application of new functional nanomaterials based on graphene and its inorganic analogues.

Hua Zhang obtained his B.S. and M.S. degrees from Nanjing University in 1992 and 1995, respectively, and completed his Ph.D. with Prof. Zhongfan Liu at Peking University in 1998. As a Postdoctoral Fellow, he joined Prof. Frans C. De Schryver's group at Katholieke Universiteit Leuven (Belgium) in 1999 and then Prof. Chad A. Mirkin's group at Northwestern University in 2001. After working at NanoInk Inc. (USA) and Institute of Bioengineering and Nanotechnology (Singapore), he joined Nanyang Technological University in 2006 and was promoted to a full professor in 2013. His current research interest focuses on two-dimensional nanomaterials including graphene and metal dichalcogenides and their applications in nano- and biosensors, clean energy, water remediation, etc.

REFERENCES

(1) Novoselov, K. S.; Geim, A. K.; Morozov, S. V.; Jiang, D.; Zhang, Y.; Dubonos, S. V.; Grigorieva, I. V.; Firsov, A. A. Electric Field Effect in Atomically Thin Carbon Films. *Science* **2004**, *306*, 666−669.

(2) Huang, X.; Yin, Z. Y.; Wu, S. X.; Qi, X. Y.; He, Q. Y.; Zhang, Q. C.; Yan, Q. Y.; Boey, F.; Zhang, H. Graphene-Based Materials: Synthesis, Characterization, Properties, and Applications. *Small* **2011**, *7*, 1876−1902.

(3) Wang, Q. H.; Kalantar-Zadeh, K.; Kis, A.; Coleman, J. N.; Strano, M. S. Electronics and Optoelectronics of Two-Dimensional Transition Metal Dichalcogenides. *Nat. Nanotechnol.* **2012**, *7*, 699−712.

(4) Song, X. F.; Hu, J. L.; Zeng, H. B. Two-Dimensional Semiconductors: Recent Progress and Future Perspectives. *J. Mater. Chem. C* **2013**, *1*, 2952−2969.

(5) Chhowalla, M.; Shin, H. S.; Eda, G.; Li, L. J.; Loh, K. P.; Zhang, H. The Chemistry of Two-Dimensional Layered Transition Metal Dichalcogenide Nanosheets. *Nat. Chem.* **2013**, *5*, 263−275.

(6) Huang, X.; Zeng, Z. Y.; Zhang, H. Metal Dichalcogenide Nanosheets: Preparation, Properties and Applications. *Chem. Soc. Rev.* **2013**, *42*, 1934−1946.

(7) Mak, K. F.; Lee, C.; Hone, J.; Shan, J.; Heinz, T. F. Atomically Thin MoS_2: A New Direct-Gap Semiconductor. *Phys. Rev. Lett.* **2010**, *105*, No. 136805.

(8) Zhao, Y.; Luo, X.; Li, H.; Zhang, J.; Araujo, P. T.; Gan, C. K.; Wu, J.; Zhang, H.; Quek, S. Y.; Dresselhaus, M. S.; Xiong, Q. Interlayer Breathing and Shear Modes in Few-Trilayer MoS_2 and WSe_2. *Nano Lett.* **2013**, *13*, 1007−1015.

(9) Tongay, S.; Zhou, J.; Ataca, C.; Lo, K.; Matthews, T. S.; Li, J. B.; Grossman, J. C.; Wu, J. Q. Thermally Driven Crossover from Indirect toward Direct Bandgap in 2D Semiconductors: $MoSe_2$ Versus MoS_2. *Nano Lett.* **2012**, *12*, 5576−5580.

(10) Splendiani, A.; Sun, L.; Zhang, Y. B.; Li, T. S.; Kim, J.; Chim, C. Y.; Galli, G.; Wang, F. Emerging Photoluminescence in Monolayer MoS_2. *Nano Lett.* **2010**, *10*, 1271−1275.

(11) Eda, G.; Yamaguchi, H.; Voiry, D.; Fujita, T.; Chen, M. W.; Chhowalla, M. Photoluminescence from Chemically Exfoliated MoS_2. *Nano Lett.* **2011**, *11*, 5111−5116.

(12) Li, H.; Qi, X. Y.; Wu, J.; Zeng, Z. Y.; Wei, J.; Zhang, H. Investigation of MoS_2 and Graphene Nanosheets by Magnetic Force Microscopy. *ACS Nano* **2013**, *7*, 2842−2849.

(13) Yin, Z. Y.; Li, H.; Li, H.; Jiang, L.; Shi, Y. M.; Sun, Y. H.; Lu, G.; Zhang, Q.; Chen, X. D.; Zhang, H. Single-Layer MoS_2 Phototransistors. *ACS Nano* **2012**, *6*, 74−80.

(14) Lopez-Sanchez, O.; Lembke, D.; Kayci, M.; Radenovic, A.; Kis, A. Ultrasensitive Photodetectors Based on Monolayer MoS_2. *Nat. Nanotechnol.* **2013**, *8*, 497−501.

(15) Zeng, H. L.; Dai, J. F.; Yao, W.; Xiao, D.; Cui, X. D. Valley Polarization in MoS_2 Monolayers by Optical Pumping. *Nat. Nanotechnol.* **2012**, *7*, 490−493.

(16) Mak, K. F.; He, K. L.; Shan, J.; Heinz, T. F. Control of Valley Polarization in Monolayer MoS_2 by Optical Helicity. *Nat. Nanotechnol.* **2012**, *7*, 494−498.

(17) Radisavljevic, B.; Radenovic, A.; Brivio, J.; Giacometti, V.; Kis, A. Single-Layer MoS_2 Transistors. *Nat. Nanotechnol.* **2011**, *6*, 147−150.

(18) Li, H.; Yin, Z. Y.; He, Q. Y.; Huang, X.; Lu, G.; Fam, D. W. H.; Tok, A. I. Y.; Zhang, Q.; Zhang, H. Fabrication of Single- and Multilayer MoS_2 Film-Based Field-Effect Transistors for Sensing No at Room Temperature. *Small* **2012**, *8*, 63−67.

(19) Bertolazzi, S.; Krasnozhon, D.; Kis, A. Nonvolatile Memory Cells Based on MoS_2/Graphene Heterostructures. *ACS Nano* **2013**, *7*, 3246−3252.

(20) Lee, H. S.; Min, S. W.; Chang, Y. G.; Park, M. K.; Nam, T.; Kim, H.; Kim, J. H.; Ryu, S.; Im, S. MoS_2 Nanosheet Phototransistors with Thickness-Modulated Optical Energy Gap. *Nano Lett.* **2012**, *12*, 3695−3700.

(21) Kim, S.; Konar, A.; Hwang, W. S.; Lee, J. H.; Lee, J.; Yang, J.; Jung, C.; Kim, H.; Yoo, J. B.; Choi, J. Y.; Jin, Y. W.; Lee, S. Y.; Jena, D.; Choi, W.; Kim, K. High-Mobility and Low-Power Thin-Film Transistors Based on Multilayer MoS_2 Crystals. *Nat. Commun.* **2012**, *3*, 1011.

(22) Feng, J.; Peng, L.; Wu, C.; Sun, X.; Hu, S.; Lin, C.; Dai, J.; Yang, J.; Xie, Y. Giant Moisture Responsiveness of VS_2 Ultrathin Nanosheets for Novel Touchless Positioning Interface. *Adv. Mater.* **2012**, *24*, 1969−1974.

(23) Feng, J.; Sun, X.; Wu, C.; Peng, L.; Lin, C.; Hu, S.; Yang, J.; Xie, Y. Metallic Few-Layered VS_2 Ultrathin Nanosheets: High Two-Dimensional Conductivity for In-Plane Supercapacitors. *J. Am. Chem. Soc.* **2011**, *133*, 17832−17838.

(24) Sun, Y.; Cheng, H.; Gao, S.; Liu, Q.; Sun, Z.; Xiao, C.; Wu, C.; Wei, S.; Xie, Y. Atomically Thick Bismuth Selenide Freestanding Single

Layers Achieving Enhanced Thermoelectric Energy Harvesting. *J. Am. Chem. Soc.* **2012**, *134*, 20294−20297.
(25) Sun, Y.; Cheng, H.; Gao, S.; Sun, Z.; Liu, Q.; Liu, Q.; Lei, F.; Yao, T.; He, J.; Wei, S.; Xie, Y. Freestanding Tin Disulfide Single-Layers Realizing Efficient Visible-Light Water Splitting. *Angew. Chem., Int. Ed.* **2012**, *51*, 8727−8731.
(26) Xu, K.; Chen, P.; Li, X.; Wu, C.; Guo, Y.; Zhao, J.; Wu, X.; Xie, Y. Ultrathin Nanosheets of Vanadium Diselenide: A Metallic Two-Dimensional Material with Ferromagnetic Charge-Density-Wave Behavior. *Angew. Chem., Int. Ed.* **2013**, *52*, 10477−10481.
(27) Zhang, X.; Xie, X.; Wang, H.; Zhang, J.; Pan, B.; Xie, Y. Enhanced Photoresponsive Ultrathin Graphitic-Phase C_3N_4 Nanosheets for Bioimaging. *J. Am. Chem. Soc.* **2013**, *135*, 18−21.
(28) Zhang, X.; Xie, Y. Recent Advances in Free-Standing Two-Dimensional Crystals with Atomic Thickness: Design, Assembly and Transfer Strategies. *Chem. Soc. Rev.* **2013**, *42*, 8187−8199.
(29) Huang, X.; Zeng, Z.; Bao, S.; Wang, M.; Qi, X.; Fan, Z.; Zhang, H. Solution-Phase Epitaxial Growth of Noble Metal Nanostructures on Dispersible Single-Layer Molybdenum Disulfide Nanosheets. *Nat. Commun.* **2013**, *4*, 1444.
(30) Zeng, Z.; Tan, C.; Huang, X.; Bao, S.; Zhang, H. Growth of Noble Metal Nanoparticles on Single-Layer TiS_2 and TaS_2 Nanosheets for Hydrogen Evolution Reaction. *Energy Environ. Sci.* **2014**, *7*, 797−803.
(31) Zhu, C.; Zeng, Z.; Li, H.; Li, F.; Fan, C.; Zhang, H. Single-Layer MoS_2-Based Nanoprobes for Homogeneous Detection of Biomolecules. *J. Am. Chem. Soc.* **2013**, *135*, 5998−6001.
(32) Wu, J.; Li, H.; Yin, Z.; Li, H.; Liu, J.; Cao, X.; Zhang, Q.; Zhang, H. Layer Thinning and Etching of Mechanically Exfoliated MoS_2 Nanosheets by Thermal Annealing in Air. *Small* **2013**, *9*, 3314−3319.
(33) He, Q.; Zeng, Z.; Yin, Z.; Li, H.; Wu, S.; Huang, X.; Zhang, H. Fabrication of Flexible MoS_2 Thin-Film Transistor Arrays for Practical Gas-Sensing Applications. *Small* **2012**, *8*, 2994−2999.
(34) Huang, X.; Tan, C.; Yin, Z.; Zhang, H. Hybrid Nanostructures Based on Two-Dimensional Nanomaterials. *Adv. Mater.* **2014**, DOI: 10.1002/adma.201304964.
(35) Zeng, Z. Y.; Yin, Z. Y.; Huang, X.; Li, H.; He, Q. Y.; Lu, G.; Boey, F.; Zhang, H. Single-Layer Semiconducting Nanosheets: High-Yield Preparation and Device Fabrication. *Angew. Chem., Int. Ed.* **2011**, *50*, 11093−11097.
(36) Li, H.; Lu, G.; Yin, Z. Y.; He, Q. Y.; Li, H.; Zhang, Q.; Zhang, H. Optical Identification of Single- and Few-Layer MoS_2 Sheets. *Small* **2012**, *8*, 682−686.
(37) Castellanos-Gomez, A.; Barkelid, M.; Goossens, A. M.; Calado, V. E.; van der Zant, H. S. J.; Steele, G. A. Laser-Thinning of MoS_2: On Demand Generation of a Single-Layer Semiconductor. *Nano Lett.* **2012**, *12*, 3187−3192.
(38) Lewerenz, H. J.; Heller, A.; Disalvo, F. J. Relationship between Surface-Morphology and Solar Conversion Efficiency of WSe_2 Photoanodes. *J. Am. Chem. Soc.* **1980**, *102*, 1877−1880.
(39) Tenne, R.; Wold, A. Passivation of Recombination Centers in *n*-WSe_2 Yields High-Efficiency (>14%) Photoelectrochemical Cell. *Appl. Phys. Lett.* **1985**, *47*, 707−709.
(40) Li, H.; Lu, G.; Wang, Y.; Yin, Z. Y.; Cong, C.; He, Q.; Wang, L.; Ding, F.; Yu, T.; Zhang, H. Mechanical Exfoliation and Characterization of Single- and Few-Layer Nanosheets of WSe_2, TaS_2, and $TaSe_2$. *Small* **2013**, *9*, 1974−1981.
(41) Fang, H.; Chuang, S.; Chang, T. C.; Takei, K.; Takahashi, T.; Javey, A. High-Performance Single Layered WSe_2 p-FETs with Chemically Doped Contacts. *Nano Lett.* **2012**, *12*, 3788−3792.
(42) Liu, W.; Kang, J. H.; Sarkar, D.; Khatami, Y.; Jena, D.; Banerjee, K. Role of Metal Contacts in Designing High-Performance Monolayer n-Type WSe_2 Field Effect Transistors. *Nano Lett.* **2013**, *13*, 1983−1990.
(43) Fang, H.; Tosun, M.; Seol, G.; Chang, T. C.; Takei, K.; Guo, J.; Javey, A. Degenerate n-Doping of Few-Layer Transition Metal Dichalcogenides by Potassium. *Nano Lett.* **2013**, *13*, 1991−1995.
(44) Zhao, W.; Ghorannevis, Z.; Chu, L.; Toh, M.; Kloc, C.; Tan, P. H.; Eda, G. Evolution of Electronic Structure in Atomically Thin Sheets of WS_2 and WSe_2. *ACS Nano* **2013**, *7*, 791−797.
(45) Zhan, Y. J.; Liu, Z.; Najmaei, S.; Ajayan, P. M.; Lou, J. Large-Area Vapor-Phase Growth and Characterization of MoS_2 Atomic Layers on a SiO_2 Substrate. *Small* **2012**, *8*, 966−971.
(46) Coleman, J. N.; Lotya, M.; O'Neill, A.; Bergin, S. D.; King, P. J.; Khan, U.; Young, K.; Gaucher, A.; De, S.; Smith, R. J.; Shvets, I. V.; Arora, S. K.; Stanton, G.; Kim, H. Y.; Lee, K.; Kim, G. T.; Duesberg, G. S.; Hallam, T.; Boland, J. J.; Wang, J. J.; Donegan, J. F.; Grunlan, J. C.; Moriarty, G.; Shmeliov, A.; Nicholls, R. J.; Perkins, J. M.; Grieveson, E. M.; Theuwissen, K.; McComb, D. W.; Nellist, P. D.; Nicolosi, V. Two-Dimensional Nanosheets Produced by Liquid Exfoliation of Layered Materials. *Science* **2011**, *331*, 568−571.
(47) Li, H.; Wu, J.; Huang, X.; Lu, G.; Yang, J.; Lu, X.; Xiong, Q.; Zhang, H. Rapid and Reliable Thickness Identification of Two-Dimensional Nanosheets Using Optical Microscopy. *ACS Nano* **2013**, *7*, 10344−10353.
(48) Schneider, C. A.; Rasband, W. S.; Eliceiri, K. W. NIH Image to ImageJ: 25 Years of Image Analysis. *Nat. Methods* **2012**, *9*, 671−675.
(49) Lee, C.; Yan, H.; Brus, L. E.; Heinz, T. F.; Hone, J.; Ryu, S. Anomalous Lattice Vibrations of Single- and Few-Layer MoS_2. *ACS Nano* **2010**, *4*, 2695−2700.
(50) Luo, X.; Zhao, Y.; Zhang, J.; Toh, M.; Kloc, C.; Xiong, Q.; Quek, S. Y. Effects of Lower Symmetry and Dimensionality on Raman Spectra in Two-Dimensional WSe_2. *Phys. Rev. B* **2013**, *88*, No. 195313.
(51) Daniel, M. F.; Desbat, B.; Lassegues, J. C.; Gerand, B.; Figlarz, M. Infrared and Raman-Study of WO_3 Tungsten Trioxides and WO_3, xH_2O Tungsten Trioxide Hydrates. *J. Solid State Chem.* **1987**, *67*, 235−247.
(52) Bohmisch, M.; Burmeister, F.; Boneberg, J.; Leiderer, P. Nanostructuring on WSe_2 with the Atomic Force Microscope by a Potential Controlled Electrochemical Reaction. *Appl. Phys. Lett.* **1996**, *69*, 1882−1884.
(53) Mahalu, D.; Margulis, L.; Wold, A.; Tenne, R. Preparation of WSe_2 Surfaces with High Photoactivity. *Phys. Rev. B* **1992**, *45*, 1943−1946.
(54) Zhang, X.; Han, W. P.; Wu, J. B.; Milana, S.; Lu, Y.; Li, Q. Q.; Ferrari, A. C.; Tan, P. H. Raman Spectroscopy of Shear and Layer Breathing Modes in Multilayer MoS_2. *Phys. Rev. B* **2013**, *87*, No. 115413.
(55) Tongay, S.; Varnoosfaderani, S. S.; Appleton, B. R.; Wu, J. Q.; Hebard, A. F. Magnetic Properties of MoS_2: Existence of Ferromagnetism. *Appl. Phys. Lett.* **2012**, *101*, No. 123105.
(56) Xia, F. N.; Mueller, T.; Golizadeh-Mojarad, R.; Freitag, M.; Lin, Y. M.; Tsang, J.; Perebeinos, V.; Avouris, P. Photocurrent Imaging and Efficient Photon Detection in a Graphene Transistor. *Nano Lett.* **2009**, *9*, 1039−1044.
(57) Choi, W.; Cho, M. Y.; Konar, A.; Lee, J. H.; Cha, G. B.; Hong, S. C.; Kim, S.; Kim, J.; Jena, D.; Joo, J.; Kim, S. High-Detectivity Multilayer MoS_2 Phototransistors with Spectral Response from Ultraviolet to Infrared. *Adv. Mater.* **2012**, *24*, 5832−5836.